Journal of Power Sources 243 (2013) 419–430

Contents lists available at SciVerse ScienceDirect

Journal of Power Sources

journal homepage: www.elsevier.com/locate/jpowsour

The effect of doping $(Mn,B)_3O_4$ materials as protective layers in different metallic interconnects for Solid Oxide Fuel Cells

Verónica Miguel-Pérez [a], Ana Martínez-Amesti [a,*], María Luisa Nó [b], Aitor Larrañaga [a], María Isabel Arriortua [a,*]

[a] Departamento de Mineralogía y Petrología, Universidad del País Vasco (UPV/EHU), Facultad de Ciencia y Tecnología, Sarriena S/N, 48940 Leioa, Vizcaya, Spain
[b] Departamento de Física Aplicada II, Universidad del País Vasco (UPV/EHU), Facultad de Ciencia y Tecnología, Sarriena S/N, 48940 Leioa, Vizcaya, Spain

HIGHLIGHTS

- Structural changes on $La_{0.6}Sr_{0.4}FeO_3$ occur by Cr^{3+} substitution.
- $MnCo_2O_4$ and $MnCo_{1.9}Fe_{0.1}O_4$ were deposited on metallic interconnects.
- Spinel materials avoid chromium migration.
- ASR of cells in contact with coated alloys decrease.

ARTICLE INFO

Article history:
Received 17 December 2012
Received in revised form
22 April 2013
Accepted 23 May 2013
Available online 7 June 2013

Keywords:
Solid Oxide Fuel Cell
Interconnects
Chromium poison
Protective coating layer
Electrical contact resistance

ABSTRACT

Spinel oxides with the general formula of $(Mn,B)_3O_4$ (B = Co, Fe) were used as barrier materials between the cathode and the metallic interconnect to reduce the rate of cathode degradation by Cr poisoning. The effect of doping at the B position was investigated terms of microstructure and electrical conductivity to determine its behaviour and effectiveness as a protective layer in contact with three metallic materials (Crofer 22 APU, SS430 and Conicro 4023 W 188). The analysis showed that the use of these materials considerably decreased the reactivity and diffusion of Cr between the cathode and the metallic interconnects. The protective layer doped with Fe at the B position exhibited the least amount of reactivity with the interconnector and cathode materials. The worst results were observed for SS430 cells coated with a protective layer perhaps due to their low Cr content. The Crofer 22 APU and Conicro 4023 W 188 samples exhibited very similar conductivity results in the presence of the $MnCo_{1.9}Fe_{0.1}O_4$ protective coating. As a result, these two material combinations are a promising option for use as bipolar plates in SOFC.

1. Introduction

Solid Oxide Fuel Cells (SOFCs) are promising candidates for future energy conversion due to their efficiency in generating electricity from a variety of fuels, such as hydrogen or hydrocarbon fuels [1–3]. The future of SOFC is associated with the development of new materials for application as electrolytes, electrodes and interconnects, to be operated at an intermediate temperature (IT) (600–800 °C) [4,5].

One of the main challenges in improving the performance and cost-effectiveness of SOFCs is the development of suitable interconnect materials. Typical materials used as interconnects include the following: Perovskite type ceramic materials based on doped $LaCrO_3$ for high operation temperatures (900–1000 °C) [6,7] and metallic materials for the IT-SOFC (600–800 °C) [8–10].

Metallic materials interconnect materials can replace ceramics for IT applications because of their high strength, machinability, low cost, and a thermal expansion coefficient (TEC) that is closely matched with that of the electrode material [11]. Due to their unique properties, ferritic stainless steels (FSS) and Ni, Co-based superalloys may also be good candidates as interconnects in SOFC at temperatures around 800 °C [12].

However, the evaporation of chromium from metallic interconnects may result in a deposit at the cathode/electrolyte

* Corresponding authors. Tel.: +34 946015984; fax: +34 946013500.
E-mail addresses: ana.martinez@ehu.es (A. Martínez-Amesti), maribel.arriortua@ehu.es (M.I. Arriortua).

0378-7753/$ – see front matter © 2013 Elsevier B.V. All rights reserved.
http://dx.doi.org/10.1016/j.jpowsour.2013.05.109

interface, which severely degrades the electrical properties of the cell [13–16]. A possible solution to chromium poisoning can be achieved by using an oxide protective coating that helps minimise the area-specific resistance (ASR) and act as a barrier to the migration of chromium from the metallic material to the cathode. It is important to ensure that the barriers are chemically compatible with an appropriate TEC, thermodynamically stable in both oxidising and reducing environments at the applied temperatures, and exhibit high electrical conductivity in the cathode atmosphere. In addition, these layers should have adequate strength at elevated temperatures, ease of fabrication and low cost [17,18].

The materials used as protective layers include: a) reactive element oxides (REOs) [19] such as La_2O_3, CeO_2 and Y_2O_3,, b) conductive Perovskites [20] such as $(La_xSr_{1-x})CoO_3$, $((La_{1-x}Sr_x)CrO_3)$, $(La_xSr_{1-x})MnO_3$ and $La_{0.6}Sr_{0.4}Co_{0.2}Fe_{0.8}O_3$, c) MAlCrYO (where M represents a metal, e.g., Co, Mn, Ti or Ni) [21] and d) conductive spinels, which are very promising coatings materials due to the improved electronic conductivity of the oxide [22–24].

Mn–Co spinels with the structure of $(MnCo)_3O_4$ have been studied in the literature as protective coating materials in combination with several commercial ferritic stainless steels with different Cr contents, such as Crofer 22 APU (22 %Cr), E– Brite (24% Cr), IT-11 (26% Cr), SMG232 (22% Cr). These studies concluded that the application of this material decreases the contact resistance and eliminates Cr migration towards cathode [25,26].

Other research groups [27,28], have studied Mn–Co spinels doped with Fe, Ti or Cu such as the $MnCo_{1.66}Fe_{0.34}O_4$, which exhibits higher electrical conductivity than $MnCo_2O_4$ due to a partial substitution of Co by Fe. However, the authors compared the change in the ASR of uncoated and coated interconnects, but not their contact with the cathodes.

In this study, the effect of doping $(Mn, B)_3O_4$ materials at the B position was evaluated for application as a protective layer. The chemical compatibility, Cr diffusion and mechanical stability of the metallic interconnects (Crofer 22 APU, SS430 and Conicro 4023 W 188) and the assembled layers were examined. In addition, the behaviour and effectiveness of the MC ($MnCo_2O_4$) and MCF ($MnCo_{1.9}Fe_{0.1}O_4$) were analysed using contact resistance measurements between the uncoated and coated alloys and the LSF40 cathode with a 4-point DC technique.

2. Experimental

2.1. Sample preparation

The study was performed on two pre-oxidised Fe–Cr based alloys, Crofer 22 APU (Thyssenkrupp VDM) and SS430 (Hamilton Precision Metals), and a Co based superalloy, Conicro 4023 W 188 (Thyssenkrupp VDM). The samples were oxidised in air at 800 °C for 100 h in a Carbolite furnace as described in [12]. The chemical compositions of initial alloys are provided in Table 1.

The powder materials used in this study include the following: $MnCo_2O_4$ (MC) and $MnCo_{1.9}Fe_{0.1}O_4$ (MCF10) as the protective coatings materials, $La_{0.6}Sr_{0.4}FeO_3$ (LSF40) as the cathode material, $(ZrO_2)_{0.92}$ $(Y_2O_3)_{0.08}$ (YSZ) disks with a diameter of 25 mm and a thickness of 300 μm as the electrolyte materials from NexTech, Fuel Cell Materials and $Ce_{0.8}Sm_{0.2}O_{1.9}$ (SDC) as the interlayer materials between the cathode and the electrolyte from Praxair Surface Technologies.

Table 1
Chemical composition of steel samples (in wt%) determined by ICP-AES.

	Cr	Fe	Ni	W	Co	Mn
Crofer 22 APU	22.19	77.29	–	–	–	0.52
SS430	16.77	82.79	–	–	–	0.44
Conicro 4023 W 188	22.07	2.70	22.29	15.51	36.57	0.86

For the electrochemical measurements, symmetrical half-cells (LSF40/SDC/YSZ) were prepared by wet colloidal spray deposition with a reference electrode area of 0.25 cm^2, as described in Ref. [5]. The deposition of protective coatings was performed using the same deposition technique as on the pre-oxidised interconnects, which were sintered at 1000 °C for 10 h in air. The initial suspensions were prepared by mixing the powders with a ball mill for 1 h. Ethanol and ZrO_2 cylinders (3 mm diameter) were used as the grinding media. The interconnects were prepared in the presence and absence of a spinel protective coating and the cells were stacked on top of one another. A dead weight of 1 Kg cm^{-2} was placed on top of the collection of cells to achieve better mechanical contact for conductivity measurements (Fig. 1).

The electrical conductivity of symmetrical cells was measured using the 3-point technique in air at 800 °C for 100 h using a Solartron 1260 Frequency Response Analyzer. The electronic contacts were made using platinum wire and platinum paste. To ensure good contact between the protective coating and the cathode, the surface of the cathodes was painted with a Pt paste and heated at 950 °C in air for 30 min to obtain a porous Pt contact layer. The resistance measurements were performed using a current density of 0.3 A cm^{-2}.

The samples were characterised by X-ray diffraction (XRD) at room temperature using a PHILIPS X'PERT PRO automatic diffractometer equipped with Cu K_α radiation ($\lambda = 1.5418$ Å). The power generator was set to 40 kV and 40 mA. The patterns were recorded using a 2è step of 0.026° in the 20–80° range. The preliminary identification of the composition of oxide surfaces was performed using the X`Pert HighScore Software 2003. Having identified the phases present in the samples, full-profile refinements were performed using the FULLPROF program [29–31].

The microstructure, composition analysis and phase distribution of samples following the ASR measurements were examined using a JEOL JSM-7000F scanning electron microscope (SEM) equipped with a Schottky field emission gun (FEG) and an Oxford Inca Pentafet X3 energy dispersive X-ray analyser (EDX). The EDX microanalysis was performed using backscattered electrons signal (BSE) at 20 kV and a current intensity of 1×10^{-9} A with a working distance of 10 mm. The EDX resolution was approximately 133 eV. The spectrum treatment was performed according to the procedure in Ref. [12].

For the cross-section analysis, the samples were embedded in an epoxy resin, polished using standard metallographic techniques, and coated with a coal graphite layer (10 nm) deposited by evaporation of Quorum Q150T Sputter Coater for electrical conductivity.

In this study, the Cr content is very difficult to determine using SEM analysis because the principal emission lines of Cr K_α (5.415 KeV) overlap with those of La L_β(5.385 KeV). To confirm the presence or absence of Cr in cells in contact with the uncoated and coated alloys,

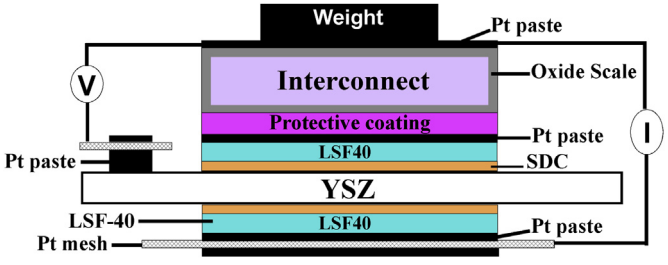

Fig. 1. Scheme of the setup for ASR measurements.

Table 2
Parameters for XPS analysis of each element.

Element	Energy range (eV)
Fe 2p	706.6–716.6
Cr 2p	574.0–581.0
O 1s	527.8–536.2
Sr $3d_{3/2}$	130.0–140.0
La $3d_{3/2}$	830.0–870.0

X-ray photoelectron spectroscopy (XPS) measurement were performed using a XPS spectrometer (SPECS). All XPS spectra were acquired using a monochromatised X-ray source producing Al K_α radiation ($h\nu = 1.486.6$ eV) and recorded using a SPECS PHOIBOS 150 analyser. The take-off angle of the photoelectrons was 90° with respect to the specimen, whereas the energy resolution was 0.6 eV. Individual high resolution spectra were obtained at 40 eV. The binding energies (BEs) were calibrated against the surface carbon contamination at 284.6 eV. The theoretical standard values of the main elements are provided in Table 2 [32,33].

3. Results and discussion

3.1. Characterisation of the protective coatings

The properties of MC and MCF10 were characterised using a variety of techniques. The purity of the samples was evaluated using X-ray diffraction analysis. Fig. 2 shows the full-profile refinement of MC ($MnCo_2O_4$) and MCF10 ($MnCo_{1.9}Fe_{0.1}O_4$) X-ray profiles obtained by fitting the Rietveld method.

Quantitative analysis reveals a single phase corresponding to the expected compounds crystallised inside the face centred cubic spinel phase with the *Fd-3m* space group [34]. A binary spinel oxide has the formula of $A[B_2]O_4$ in which A is a cation that is tetrahedrally coordinated with the oxygen whereas B is a cation that is octahedrally coordinated with the oxygen. In this case, both oxides are refined using the starting parameters from the PDF file number 23-1237. The refined cell parameters and cell unit volumes are summarised in Table 3.

Fig. 2 confirms that samples are pure and that MCF10 exhibits higher crystallinity than MC. The increase in the cubic cell parameter of MCF10 can be attributed to the substitution of Fe cations into the Co sites.

The powder morphology was examined to determine the distribution of particle size and the homogeneity of each sample (Fig. 3).

The powders are homogenous and exhibit similar morphology in terms of particle size distribution with an average grain size of 0.25–1 μm and 1–2 μm for MC and MCF10, respectively.

Table 3
Structural parameters obtained from the Rietveld refinement.

Protective coating	Space group	Lattice parameters		
		a (Å)	V (Å^3)	R_{Bragg} (%)
MC	*Fd-3m*	8.2605(3)	563.67(5)	5.82
MCF10	*Fd-3m*	8.2955(5)	570.84(6)	5.12

The total conductivity measurements of MC and MCF10 powders were performed in air using a four-probe DC technique from room temperature to 950 °C at a heating rate of 3 °C min^{-1}. The samples were prepared by pressing 1 g of the protective powders with 2 tons of force for 1 min using a Specac uniaxial press with a 13 mm diameter. Pellets were sintered in a conventional Carbolite tubular furnace at 1200 °C in air for 20 h using a heating rate of 3 °C min^{-1}. The sintered pellets were cut and polished into small rectangular bars with approximate dimensions of 1 × 3 × 10 mm. Pt paste and electrode leads were placed over the polished surfaces to create electrical contact points (Fig. 4). The ASR (Ω cm^{-2}) of the coating materials was calculated using Ohm's Law (Eq. (1)):

$$ASR = \frac{V}{I} \tag{1}$$

where V is the voltage drop and I is the current density.

The electrical conductivity σ (S cm^{-1}) was obtained using Eq. (2):

$$\sigma = \left[\frac{L}{A \times R}\right] \tag{2}$$

where R (Ω) is the measured resistance, A (cm^2) is the cross sectional area and L is the distance between the voltage contacts. The obtained conductivity values shown in Fig. 5a were corrected using the following porosity correction relation [35] (Eq. (3)):

$$\sigma_{corrected} = \sigma_{measured}\left(1 + \frac{pf_{vol}}{1 - (pf_{vol})^{2/3}}\right) \tag{3}$$

where pf_{vol} is the pore volume fraction (Eq. (4)) and $[\rho_{exp}/\rho_{theor}]$ is the ratio of experimental and theoretical densities obtained from the geometrical dimensions and the X-ray powder diffraction analysis (Fig. 2).

$$pf_{vol} = 1 - \left(\frac{\rho_{exp}}{\rho_{theor}}\right) \tag{4}$$

The experimental densities of sintered MC and MCF10 bars were 96% and 97% of the theoretical densities, respectively.

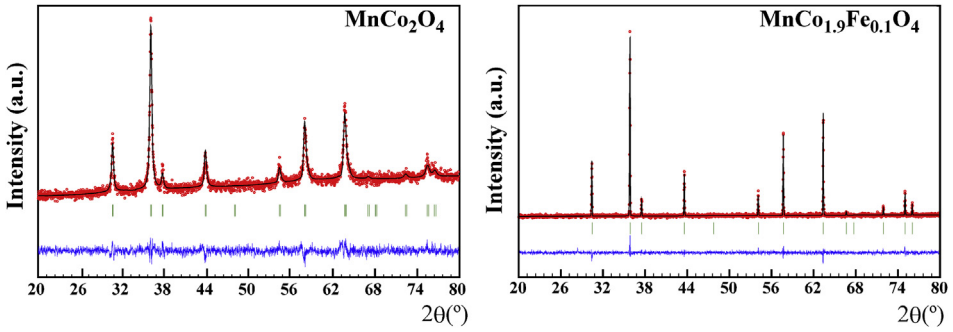

Fig. 2. Full-profile X-ray refinements of MC and MCF10. The experimental and calculated intensity data are plotted as dotted and solid lines, respectively, and the difference ($I_{exp} - I_{cal}$) is shown as the lower solid line.

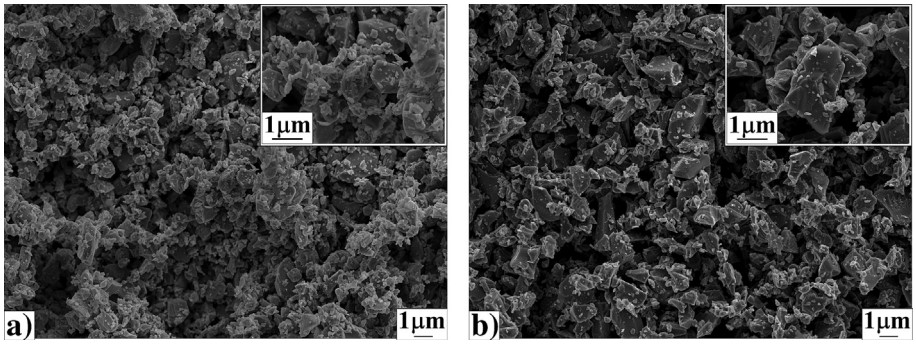

Fig. 3. SEM micrographs of the surface of: (a) MC and (b) MCF10 powders.

Fig. 5b shows the conductivity dependence as a function of inverse temperature, as described by Eq. (5):

$$\sigma = \frac{\sigma_0}{T}\exp\left(-\frac{E_a}{kT}\right) \quad (5)$$

where σ is the conductivity, E_a is the activation energy, T is the absolute temperature, k is the Boltzmann constant and σ_0 the pre-exponent factor related to the concentration of charge carriers.

The experimental values of the electrical conductivity are expected to correspond to the electronic conductivity. The electrical conductivity of MC and MCF10 increases with increasing temperature (Fig. 5a). The electrical conductivity values of MC and MCF10 were 67 and 72 S cm^{-1} at 800 °C in air, respectively, and the E_a values were estimated to be 0.44 eV and 0.38 eV, respectively (Fig. 5b). When Co is substituted with Fe, the conductivity increased due to the presence of mixed valence states at the B site of the spinel structure.

It is difficult to determine the cation distribution in cobalt and manganese oxide spinels because of the variety of possible oxidation states for both elements [36]. The most probable cationic distribution of Mn–Co spinels reported in the literature indicates that the tetrahedral sites in the unit formula are occupied by Co^{2+} and Mn^{2+} ions, whereas Co^{2+}, Co^{3+}, Mn^{3+} and Mn^{4+} ions occupy the octahedral sites, according to the following formula: $Co^{2+}Mn^{2+}$ [$Co^{2+}Co^{3+}Mn^{3+}$ Mn^{4+}] [37,38].

By taking into account the proposed formula for MC and literature description of spinel ferrites [M^{2+} Fe^{3+}]([M^{2+}, Fe^{2+}, Fe^{3+}]O_4, where M represents metallic cations, the following cationic distributions for MCF10 are proposed herein: (Co^{2+},Mn^{2+},Fe^{3+})(Co^{2+}, Co^{3+}, Mn^{3+}, $Mn^{4+}Fe^{2+}$, Fe^{3+})$_2O_4$ [39,40].

The activation energy of MCF10 is lower than that of MC. This finding indicates that the movement of charge carriers is more facile in MCF10 than in MC, resulting in a higher electronic conductivity of MCF10. These results are in good agreement with previous studies [28].

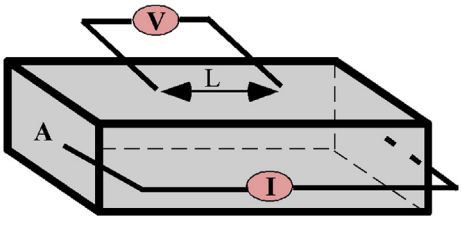

Fig. 4. Scheme of the setup for electrical conductivity of coating material by the 4 point DC technique.

3.2. Compatibility between the protective layers and the metallic interconnect

The chemical compatibility between the protective coating layers and pre-oxidised metallic interconnects were examined after oxidation at 800 °C for 100 h in air. Fig. 6 shows the X-ray patterns obtained at room temperature for substrates coated with MC and MCF10 protective coatings after oxidation in air at 800 °C for 100 h. These X-ray patterns are compared with the X-ray pattern of each pre-oxidised alloy as well as the MC and MCF10 X-ray powder patterns.

The oxide portion of the alloys oxidised in air at 800 °C for 100 h was composed of a double-layer structure: the inner layer was formed mainly of chromia (Cr_2O_3) and the outer layer was composed of $(Fe,Cr,Mn)_3O_4$ for Crofer 22 APU and SS430, and/or $(Co,Cr,Mn)_3O_4$ for Conicro 4023 W 188. In addition to the secondary phases, a series of peaks was observed due to the substrate: Fe–Cr peaks for Crofer 22 APU, SS430 and Co–Ni–Cr peaks for Conicro 4023 W 188. Quantitative analysis of oxidised alloys is described in Ref. [12].

No secondary phases were observed in the protective layers after oxidation in air at 800 °C for 100 h for the Crofer 22 APU and Conicro 4023 W 188 substrates. However, a reaction between the oxide scale of SS430 and the protective layers was observed.

In addition, a slight shift to a lower 2θ angle was observed for MC and MCF10 peaks in contact with Crofer 22 APU, SS430 and Conicro 4023 W 188. This effect indicates that the original protective layers exhibits a lower increase in the unit cell volume than Conicro 4023 W 188/MCF10. To quantify the unit cell volume variation, a full-profile X-ray refinement was performed (Table 4).

The unit cell volume variation is related to the partial substitution of Cr at the B position by Mn and/or Co in the case of $MnCo_2O_4$, and Fe in the case of MCF10. By taking into account the atomic radii of the elements that form the spinel material, the following arrangement is proposed: (Co^{2+} 0.65 Å (N.C = 6); Co^{3+} 0.61 Å (N.C = 6); Mn^{3+} 0.64 Å (N.C = 6); Mn^{4+} 0.53 Å (N.C = 6); Fe^{3+} 0.64 Å (N.C = 6) and Fe^{4+} 0.58 Å (N.C = 6)) with Cr^{3+} 0.62 Å (N.C = 6) [41].

This replacement is possible, and because Cr atoms are bigger than those replacing it at the B position in $MnCo_2O_4$ and $MnCo_{1.9}Fe_{0.1}O_4$, the unit cell volume should increase. The described process can form phases such as $Mn_{0.4}Co_{0.6}Cr_2O_4$, $MnCoCrO_4$ and $Mn(Co, Fe, Cr)_2O_4$ [28], which exhibit lower electrical conductivity than the oxides compounds formed after the oxidation of uncoated alloy surfaces. The degree of replacement is higher in MC coatings, indicating that this material is more unstable than MCF10. The presence of Fe prevents Cr from occupying the B site in the spinel structure.

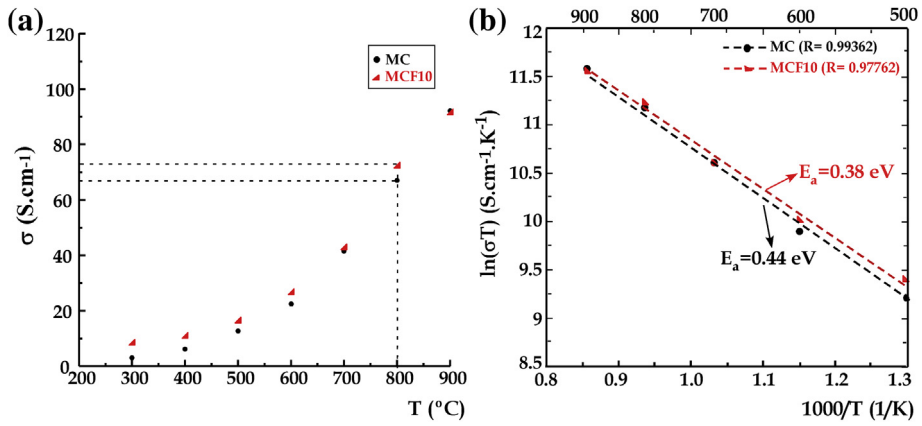

Fig. 5. (a) Temperature dependence of electrical conductivity and (b) Arrhenius plot of the electrical conductivities of protective layers.

In contrast, oxides formed at the MC/SS430 interfaces contain Cr_2O_3 and Fe_2O_3 layers. Fe_2O_3 is less dense than Cr_2O_3 and may facilite the cation diffusion of Cr^{3+}, Mn^{2+} and Fe^{3+} to the surface, resulting in a reaction with the spinel coating. However, the MCF10/SS430 interface contains $(Fe, Cr, Mn)_3O_4$ and Fe_2O_3. The possible diffusion of Cr^{3+} in the spinel protective coating to SS430 is also confirmed by the identical position of diffraction peaks of Cr_2O_3 and the pre-oxidised substrate, as shown in Fig. 6. At the same time, the peak position of the spinel is shifted to a lower angle. The increase in the unit cell volume can be attributed to the substitution of Cr cations at the Co site. The growth of new phases such as $(Mn,Co,Cr)_3O_4$ depends on the diffusion of Mn, Co, O and Cr ions, as well as the interaction between these elements, which is in good agreement with other studies [42,43].

The surface microstructure of alloys coated with MC and MCF10 after oxidation in air at 800 °C for 100 h was analysed to determine the morphology of the MC and MCF10 after the heat treatment (Fig. 7).

The surface microstructure of all samples was similar, revealing spinel particles with an average particle size of approximately 1–2 μm. However, the surface of SS430 coated with $MnCo_2O_4$ contained two different oxide particles morphologies, which corresponds to a mixture of substrate oxides and the protective layer. This result indicates that $MnCo_2O_4$ layer on top of SS430 became delaminated after the heat treatment. Thus, the secondary phases that were detected by X-ray diffraction correspond to the oxides that form on the oxide scale of the pre-oxidised alloy.

To determine the microstructure and Cr distribution along the MC and MCF10 layers, EDX line scan analysis was performed on the cross-section of the coated interconnects (Crofer 22 APU, SS430 and Conicro 4023 W 188) following oxidation in air at 800 °C for 100 h (Fig. 8).

The SEM analysis confirms that the spinel layer exhibited excellent bonding with the Crofer 22 APU and Conicro 4023 W 188 substrates, which was free of spallation or cracks. Four layers can be distinguished in the coated alloys, including: the substrate (I), the oxide scale (II), the protective layer (III) and the Pt paste (IV). The distributions of the chemical compositions in the coated alloys following the oxidation test were determined by EDX analysis. A smooth continuous interface (II) was observed between the protective layer (III) and the substrate (I). The EDX line scan reveals that zone II (with a thickness of approximately 2 μm) is composed mainly of Cr, O and some Mn. The EDX analysis provides no evidence for Cr penetration though the spinel coating in Crofer 22 APU and Conicro 4023 W 188. However, the protective layer thickness on the SS430 substrate is lower than that of other metallic materials. This result is due to a loss in adherence between the protective layer and the SS430 after the oxidation test, which is a consequence of the greater degree of Cr evaporation and a lower degree of reaction area formation that results in spallation. These findings are in good agreement with the results observed in Fig. 7.

All these processes can be explained taking into account the fact that SS430 has the lowest content of Cr and other reactive elements (Mn, W, Si, Cu, Al, La, and Ti). The X-ray diffraction and SEM analysis results demonstrate that MCF10 ($MnCo_{1.9}Fe_{0.1}O_4$) is more stable than MC ($MnCo_2O_4$) and less reactive with the selected alloys.

Because the microstructure of both layers is porous with a similar pore distribution, the addition of Fe to the spinel at the B position does not appear to have an effect on the microstructure.

3.3. *Effectiveness of protective coatings*

The room temperature X-ray diffraction pattern of the top of the cell was obtained in air after making contact with the metallic material (Crofer 22 APU, SS430 and Conicro 4023 W 188) in the presence and absence of MC and MCF10 at 800 °C for 100 h. The results are provided in Fig. 9.

The X-ray diffraction patterns of cells (1–3) confirm the interaction between the LSF40 perovskite and the uncoated metallic interconnects. In addition to the peaks observed for the materials that comprise the cells (LSF40, SDC and YSZ), there are also additional peaks in the patterns.

The $SrCrO_4$ phase is identified by the reaction of between Sr from the LSF40 cathode and Cr from the alloy/oxide. There are also peaks that may be related to the La_2O_3 and Cr_2O_3 phases. In addition, the peak near 32° gradually shifts to higher angles with decreasing Sr content. The formation of secondary phases including $SrCrO_4$, La_2O_3 and Cr_2O_3 inhibit the cathodic oxygen reduction at the triple phase boundary (TPB), which may increase the electrical resistance [14,44].

In contrast, the XRD analyses of the cells a and b do not reveal additional secondary reaction phases due to the introduction of MC and MCF10 materials as a protective layer to eliminate the reaction between the interconnect and the cathode. A slight shift to a higher angle is observed for the ferrite peaks after they come in contact with the MC-coated Crofer 22 APU and Conicro 4023 W 188, and a slight shift to a lower angle in the case of MC coated SS430. The difference in the X-ray structure corresponds to a change in the unit cell parameters, which was calculated by quantifying the displacement of peaks from the $MnCo_2O_4$ coating using the X-ray refinement software. The ferrite exhibited a 0.29% decrease in the

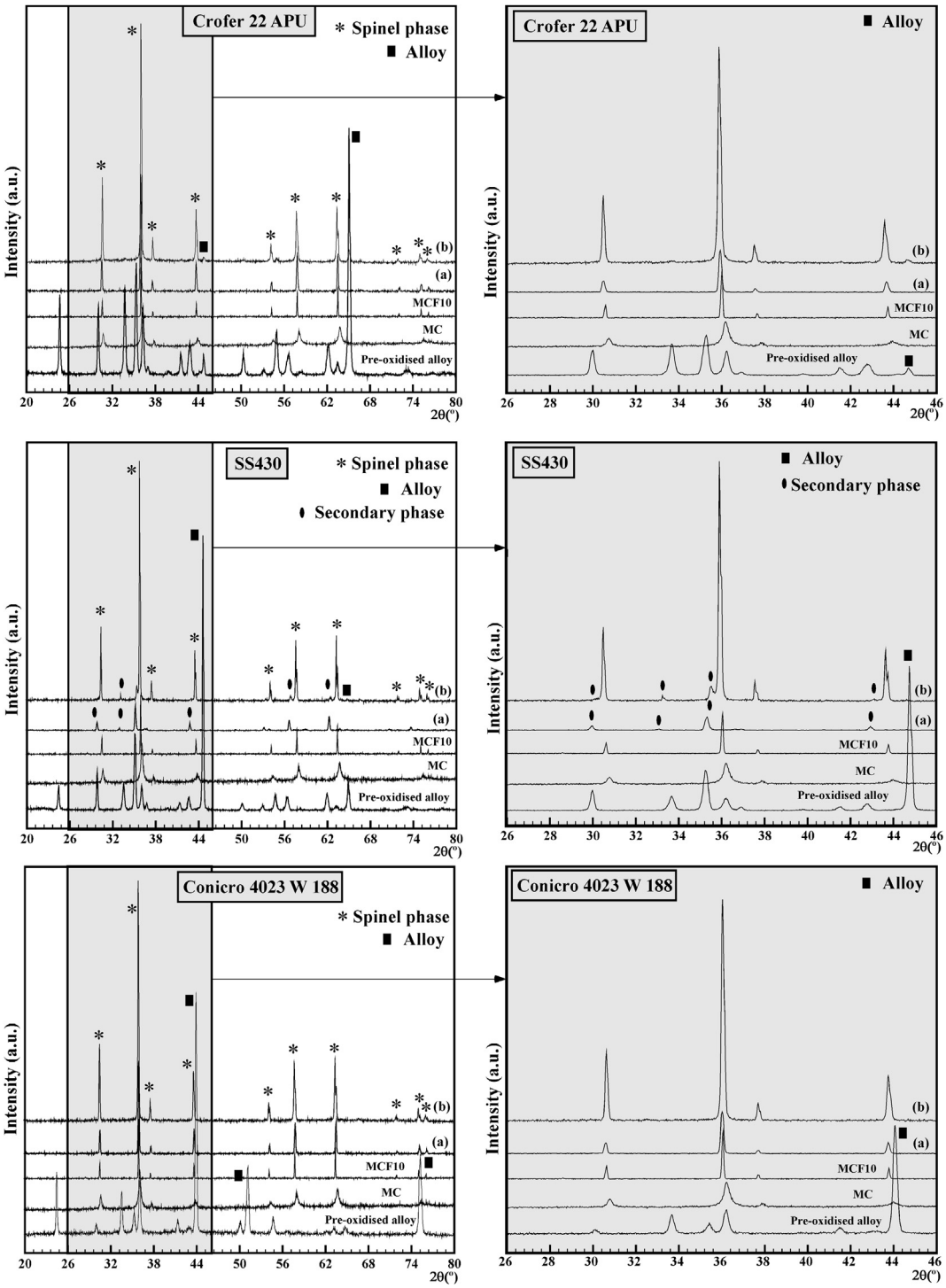

Fig. 6. XRD patterns of pre-oxidised interconnect $MnCo_2O_4$ and $MnCo_{1.9}Fe_{0.1}O_4$ powders and the assembled interconnects (Crofer 22 APU, SS430 and Conicro 4023 W 188) coated with: a) MC and b) MCF10 after oxidation in air at 800 °C for 100 h.

Table 4
Lattice parameters of the protective coating and identified phase data of coated alloys after oxidation in air at 800 °C for 100 h.

Protective layer	MC			MCF10		
Samples	Crofer 22 APU	SS430	Conicro 4023 W 188	Crofer 22 APU	SS430	Conicro 4023 W 188
Lattice parameter *a* (Å)	8.2878(2)	8.4119(1)	8.2838(1)	8.3198(1)	8.2973(1)	8.2937(1)
Secondary phases	–	Cr_2O_3 Fe_2O_3	–	Cr_2O_3	$(Fe,Cr,Mn)_3O_4$ Fe_2O_3	–
% Δ*V*	0.99	5.60	0.85	0.88	0.07	−0.06

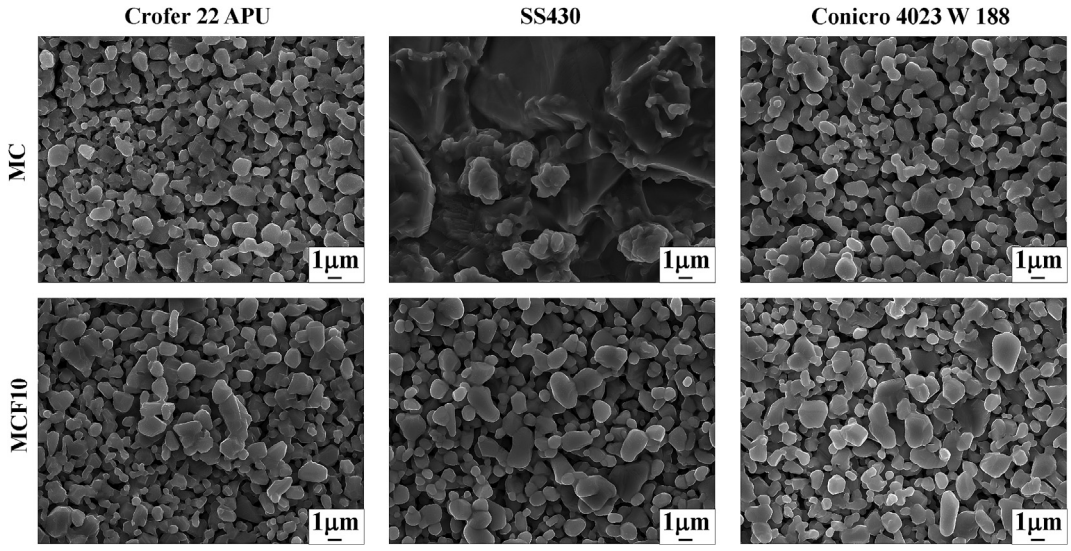

Fig. 7. SEM micrographs of Crofer 22 APU, SS430 and Conicro 4023 W 188 coated with $MnCo_2O_4$ and $MnCo_{1.9}Fe_{0.1}O_4$ after oxidation at 800 °C for 100 h in air.

unit cell volume for the LSF40 in contact with the coated Crofer 22 APU. However, the ferrite peak exhibited a 0.19% and 0.14% decrease in the unit cell volume of LSF40s in contact with Crofer 22 APU and Conicro 4023 W 188 coated with $MnCo_{1.9}Fe_{0.1}O_4$, respectively.

The observed decrease in the volume was in good agreement with the partial substitution of Fe ferrites by Mn and/or Co in the coating layer. These elements have the following atomic radii: Co^{2+}: 0.65 Å (N.C = 6); Co^{3+}: 0.61 Å (N.C = 6); Mn^{3+}: 0.64 Å (N.C = 6); Mn^{4+}: 0.53 Å (N.C = 6); Fe^{3+}: 0.64 Å (N.C = 6) and Fe^{4+}: 0.58 Å (N.C = 6)) [41]. Because replacement is possible and the replaced atoms are smaller than the ones incorporated in the ferrites, the unit cell volume is reduced.

The EDX elemental line distribution across the interface of the cells oxidised in air for 100 h at 800 °C and then placed in contact with the MC and MCF10 coated metallic interconnect are provided in Fig. 10.

For cells in contact with MC- and MCF10-coated Crofer 22 APU and SS430 samples, four areas can be distinguished. For all samples, area I is the electrolyte (YSZ), area II is the interlayer (SDC), area III is the cathode (LSF40) and area IV is the Pt paste used to make the electrical contact. The EDX analysis did not show any penetration of chromium through the cells in contact with coated metallic interconnects (Fig. 10).

To verify that Cr diffusion actually takes place through the LSF40 cathode, the surface of the cell was investigated by XPS. Fig. 11 provides the high-resolution Cr 2p XPS spectra. All the core-level intensities were corrected for XPS sensitivity factors and were plotted as a function of the binding energy (BE). Clearly, the BE coincides well with the standard values of Cr (Table 2). The Fe-2p and La-3d spectra are not shown because there were only minor differences observed between the samples.

The most obvious difference between the uncoated and coated alloys is shown in the Cr 2p region (Fig. 11). The main difference detected by XPS is in the intensity of the chromium signal. This region can be fit with two separate peak components. For all metallic interconnects, the XPS spectra show a doublet near the BEs of ~579.0 and 589.3 eV (Cr $2p_{3/2}$ level), which suggests the presence of Cr^{6+}. However, the lower BE positions of 576.5 and 586.6 eV correspond to Cr^{3+}. The +6 valence of the Cr ion in uncoated samples indicates the existence of segregated phases such as CrO_3 or $SrCrO_4$ [45], whereas the +3 valence corresponds to the Cr of the chromia (Cr_2O_3) phase. The content of CrO_3, $SrCrO_4$ and Cr_2O_3 phases was too low to be detected by XRD and SEM/EDX. Furthermore, some Cr was observed on the surface of the cathode, which did not migrate across the layer.

3.4. ASR measurements

The electrical performance of the spinel protection layer based on Crofer 22 APU, SS430 and Conicro 4023 W 188 was evaluated using ASR measurements performed in air at 800 °C for 100 h. Prior to the resistance test, the metallic interconnects were pre-oxidised in air at 800 °C for 100 h to avoid direct contact between the Pt-mesh and the metallic material [46].

Fig. 12 shows the contact ASR as a function of time at 800 °C in air for select metallic materials coated with MC and MCF10 protective layers and the resulting cell (LSF40/SDC/YSZ) (with Pt as the electrical contact paste), as well as those of the uncoated Crofer 22 APU, SS430 and Conicro 4023 W 188 interconnects.

The contact ASR of bare Crofer 22 APU, SS430 and Conicro 4023 W 188 cells increases to 0.77, 0.350 and 0.046 $\Omega \cdot cm^2$ after treatment in air for 100 h, respectively. This may be due to cathode poisoning with Cr, which contributes to a decrease in conductivity. However, the ASR of the cell assembled with the uncoated Conicro 4023 W 188 (Cell 3) interconnects also increases to 0.098 $\Omega \cdot cm^2$ after 20 h, and then decreases to 0.046 $\Omega\ cm^2$. This effect may be due to the formation of Cr_2O_3 and $(Co,Cr,Mn)_3O_4$ oxides in Conicro 4023 W 188 [12], which are more electrically conductive than the Cr_2O_3 and $(Fe,Cr,Mn)_3O_4$ phases formed on Crofer 22 APU and SS430. The overall ASR values are determined by the initial ASR and the change in ASR over time – both of which are dependent on the electronic and ionic conductivity, the oxidation resistance of the substrate metal, the oxide subscale properties and the possible interfacial interactions between the cell and the coated and uncoated metallic materials.

W. Qu et al. [19] demonstrated that the Co-containing spinel phases exhibit high conductivity values. The formation of a $CoCr_2O_4$ phase on the oxide scale of Conicro 4023 W 188 resulted in a decrease in a conductivity compared with Crofer 22 APU and SS430. The oxide formed by $MnCr_2O_4$ and chromia exhibited an order of magnitude higher resistivity than $CoCr_2O_4$. In addition, Conicro 4023 W 188 exhibited a higher Mn content compared with Crofer 22 APU and SS430. Further, Conicro 4023 W 188 revealed the formation of Laves phases, which can improve electrical properties.

In contrast, the use of Crofer 22 APU and Conicro 4023 W 188 with MC and MCF10 as the spinel protective layer resulted in a

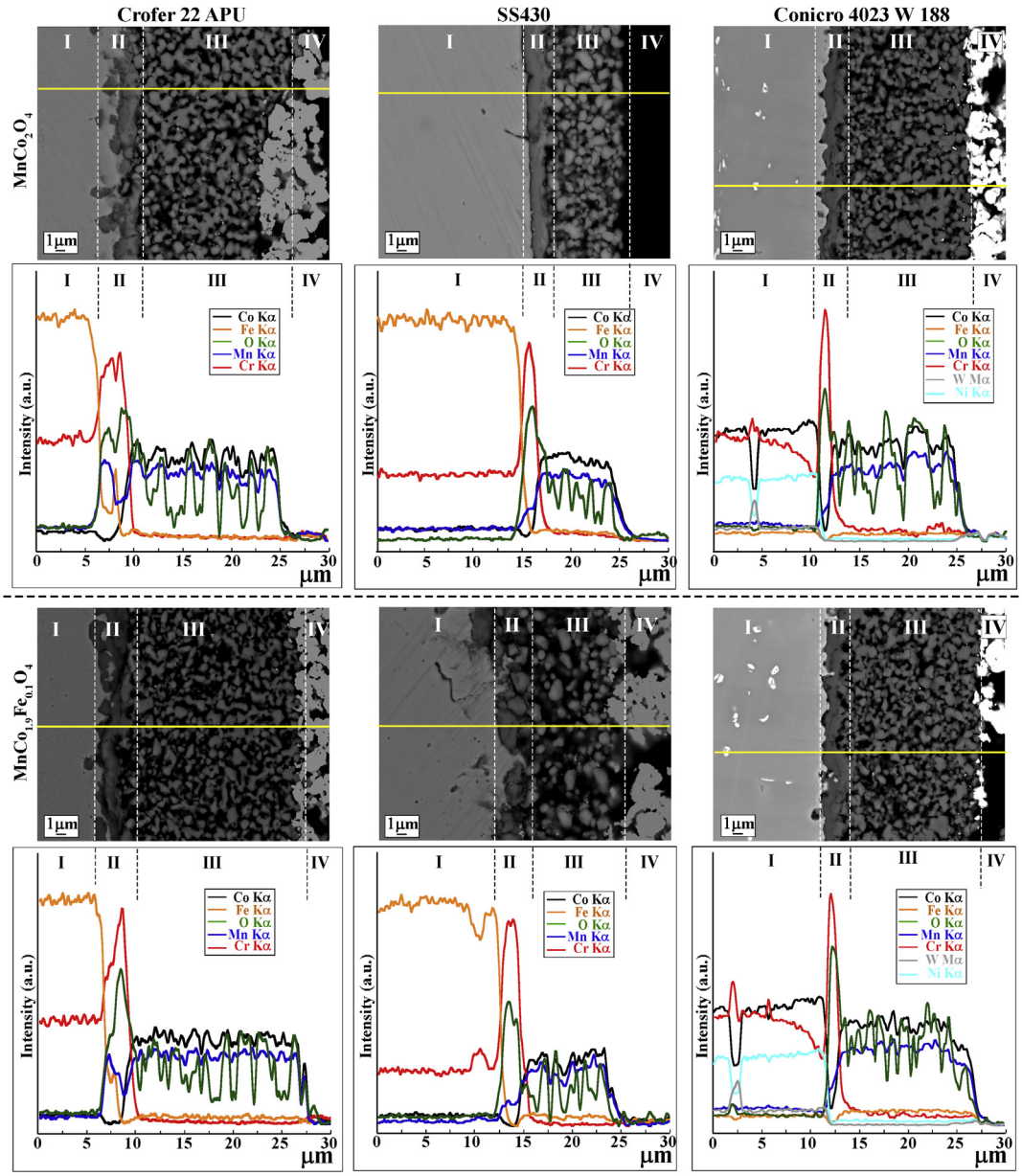

Fig. 8. Cross-sectional BSE images and the corresponding EDX elemental line scans of Crofer 22 APU, SS430 and Conicro 4023 W 188 coated with MC and MCF10 spinel after oxidation in air at 800 °C for 100 h. The acquisition parameters for the line scan were as follows: 20 kV, 25% dead time, and 5 steps with 77 s/step.

lower contact ASR. Indeed, as shown in Fig. 12, when SS430 was coated with MC, the initial ASR was even higher than that of the bare metal. This effect is attributed to the formation of a subscale on the SS430 substrate comprised of a (Mn, Cr)$_3$O$_4$ spinel layer and a chromia sub-layer. These observations are in good agreement with the SEM/EDX and XRD results.

The lowest and highest ASR values were observed for Crofer 22 APU and SS430 due to the reaction between the protective layer and the chromium species. The greatest ASR reduction was observed for the coated Crofer 22 APU material, which may be due to the generation of the MnCoCrO$_4$ spinel phase. This phase exhibits approximately a two orders of magnitude increase in the electrical conductivity relative to Cr_2O_3 and helps decrease the electrical resistance. A lower reduction in the ASR was observed between the coated and uncoated Conicro 4023 W 188. This result is attributed to the lower diffusion cation and the formation of Laves phases in the oxide scale.

Moreover, MC and MCF10 spinel protective layers on selected metallic materials (Crofer 22 APU, SS430 and Conicro 4023 W 188) act as a barrier to the diffusion of Cr cations from the surface of the interconnects through the cathode material. The decrease in Cr migration and ASR resulted in the improved electrochemical performance of the cell with a protected current collector. In all cases, the use of the MCF10 protective layer improves the ASR results. The reduction in the ASR of cells prepared with MCF10 as a protective coating is due to the presence of Mn(Co, Fe, Cr)$_2$O$_4$, which was formed at the interface between MCF10 and the interconnects. This compound exhibits higher electrical conductivity than the MnCoCrO$_4$ spinel phase generated by the Cr migration from the steel in contact with the MnCo$_2$O$_4$ coating [28,43].

The lower reactivity and dispersion of elements between the MCF10/interconnect and the LSF40 indicate that the conductivity increases. The low Fe content in the spinel coating produced a more stable Mn–Co spinel material with a higher electrical conductivity

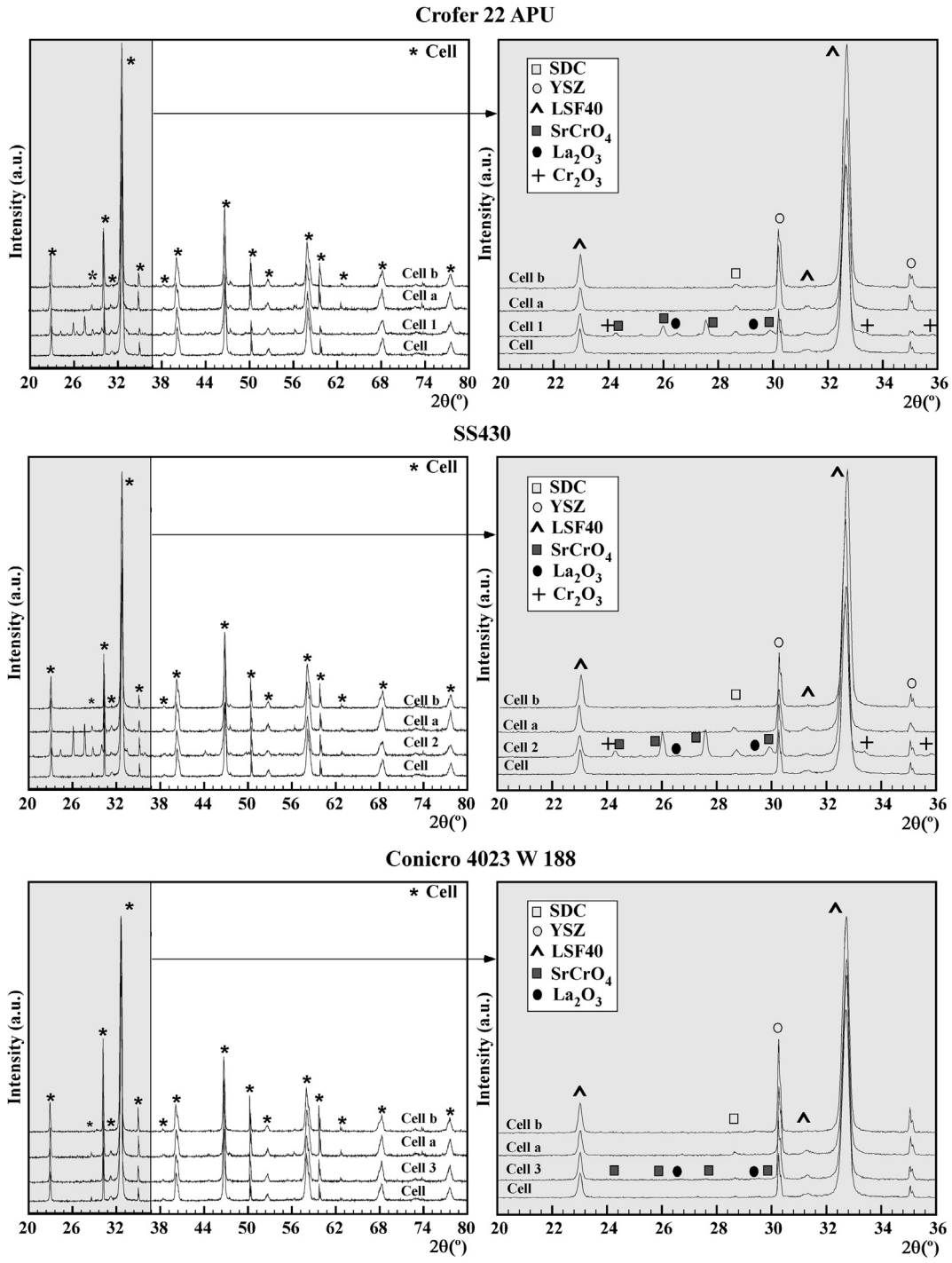

Fig. 9. Room temperature X-ray diffraction patterns of YSZ/SDC/LSF40 cells in contact with the following interconnects: uncoated Crofer 22 APU (cell 1), SS430 (cell 2) and Conicro 4023 W 188 (cell 3) and coated with MC (cell a) or MCF10 (cell b) after oxidation at 800 °C for 100 h in air.

and lower energy activation than the sample without the Fe. Because conduction in spinels occurs by change hopping between cations at the octahedral sites, the presence of different valence states among the octahedral cations is beneficial to conduction. This effect may be the reason for the improved conductivity of the MCF10 sample.

The low interfacial ASR and its decreasing trend are mainly attributed to the high electrical conductivity of the manganese cobaltite spinel, the mitigated growth of the subscale and possible interfacial interactions with the contact during the test.

The oxide scale growth of the different interconnect materials observed in Ref. [12] depends on the Cr concentration and the amount of reactive elements such as Mn, W, Si, Cu, Al, La, and Ti. In SS430, the lower Cr content compared with that of the other two ferritic stainless steels, Crofer 22 APU and Conicro 4023 W 188, resulted in the lower Cr activity at the coating/metal interface, leading to a slow formation of a continuous thin chromia sub-layer. This effect explains the higher amount of Cr diffusion through the cathode material and the spallation of the oxide scale. Indeed, the oxidation mechanism depends on the initial composition of the substrate.

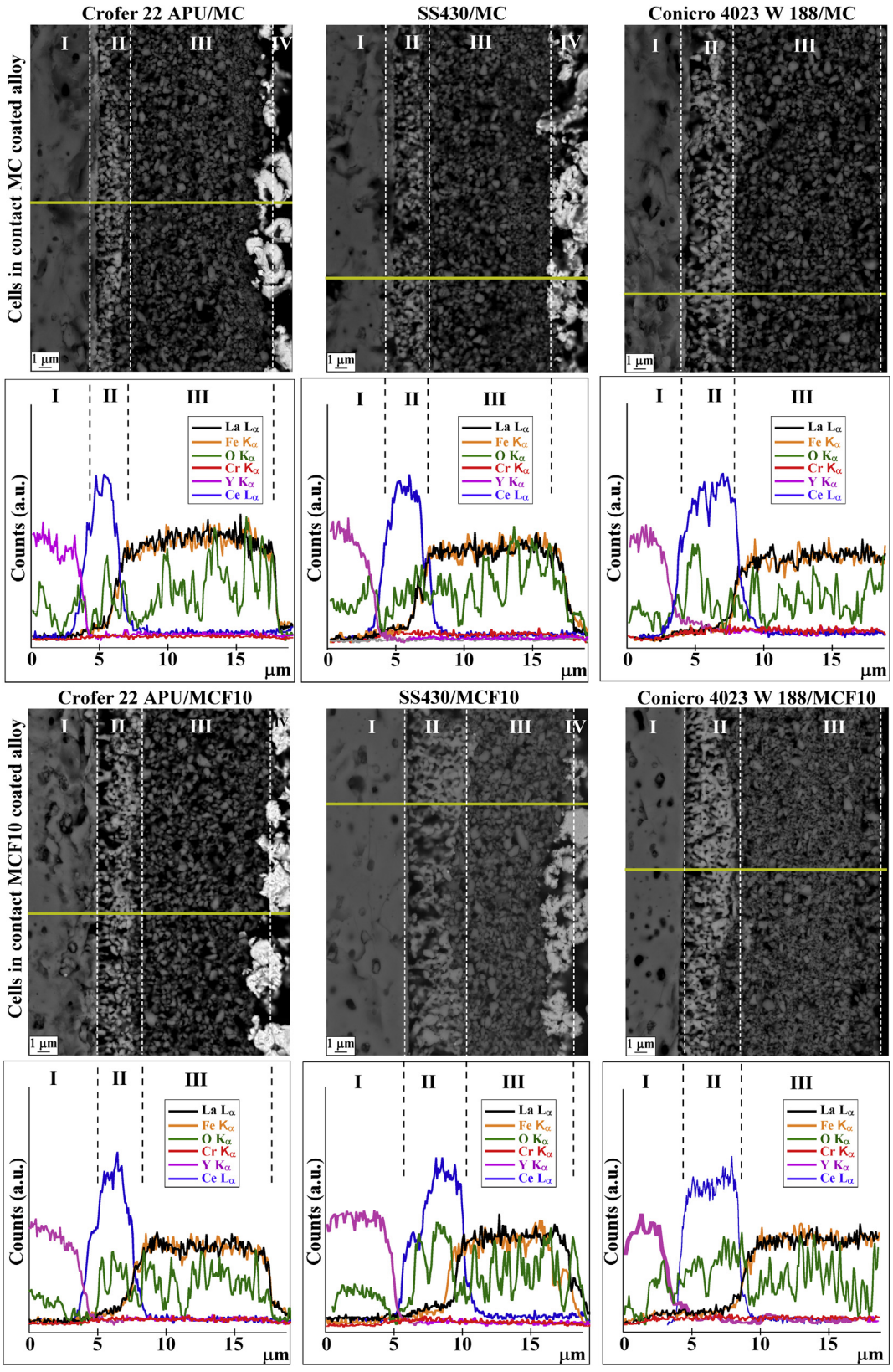

Fig. 10. Cross-sectional BSE images and the corresponding EDX elemental line scan of LSF40 in contact with alloys that were coated with MC and MCF10 after oxidation at 800 °C in air for 100 h. The acquisition parameters for the line scans were as follows: 20 kV, 25% dead time, and 5 steps with 77 s/step.

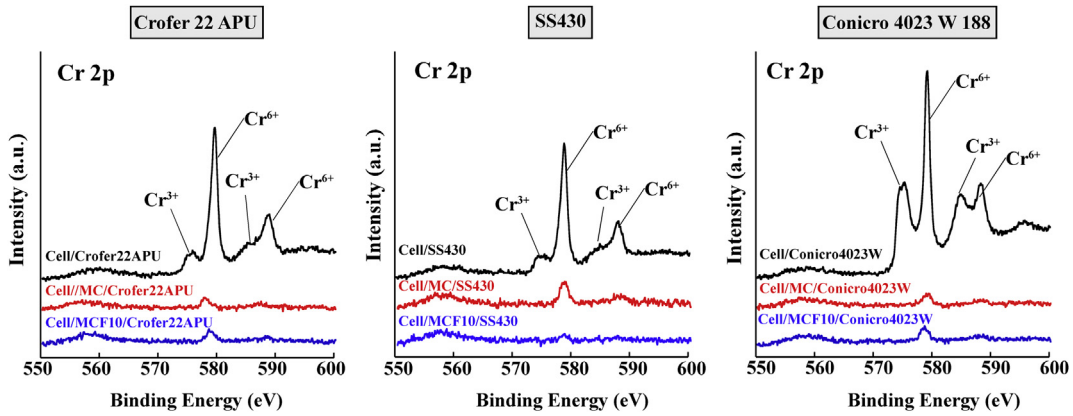

Fig. 11. XPS spectra of Cr 2p in cells surface in contact with uncoated and coated interconnects after oxidation at 800 °C for 100 h in air.

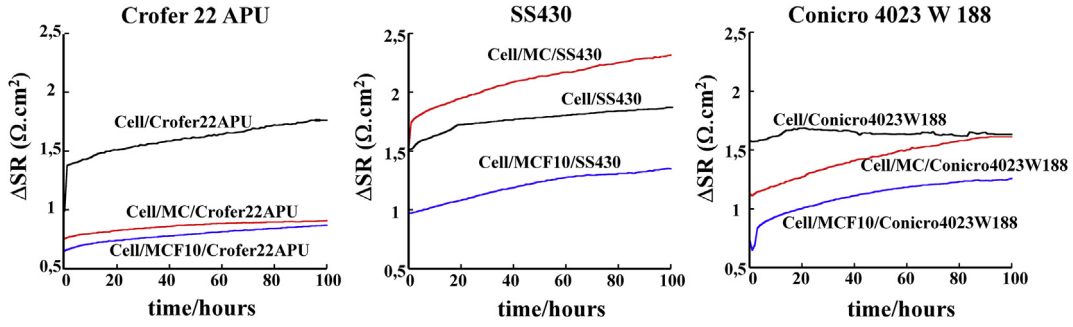

Fig. 12. ASR measurement at 800 °C for 100 h in air of cells prepared using Crofer 22 APU, SS430 and Conicro 4023 W 188 interconnects in the absence and presence of with MC and MCF10.

All interconnects prepared with the MCF10 coating exhibited a lower ASR and a lower amount of LSF40 cathode degradation. This finding could be related to the change in the transport properties of $MnCo_2O_4$ spinel due to doping with Fe ions of different valences and/or site (octahedral/tetrahedral) preferences [47]. The addition of iron to the Mn–Co spinel coating resulted in a decrease in the reaction layer, which reduced the scale spallation and improved the long term stability.

A decrease in the unit cell volume of LSF40 was observed when it came into contact with MC and MCF10. The effect was greater for LSF40 in contact with MC than MCF10. One possible reason for this difference is that the MC has a higher possibility of Fe cations occupying the octahedral sites. The diffusion of Fe in MC can affect the coating composition and the resulting electrical properties. Puranen et al. [48] found that when using an iron doped Mn–Co based oxide spinel, it is possible to improve the electrical and mechanical properties of the coatings.

At the same time, possible interactions between the oxide scale and the MC and MCF10 have been found, including the formation of $MnCoCrO_4$ and $MnCoFeCrO_4$, respectively. $MnCoFeCrO_4$ exhibits a higher electrical conductivity than $MnCoCrO_4$.

4. Conclusions

This work describes the effect of two protective layers on three alloys, which were used as metallic interconnects in SOFCs. Manual spraying was used as the coating technique for the deposition of $MnCo_2O_4$ and $MnCo_{1.9}Fe_{0.1}O_4$, which were then sintered at 1000 °C for 10 h in air. The degradation of cells in the presence of the uncoated and coated interconnects was compared at 800 °C for 100 h in air. The following results were obtained:

1) When uncoated alloys are used, secondary phases such as $SCrO_4$, Cr_2O_3 and La_2O_3 are observed due to a reaction between Cr and the cathode material. However, when the coated metallic material was in the form of $MnCo_2O_4$ (MC) and $MnCo_{1.9}Fe_{0.1}O_4$ (MCF10) spinel oxides are used, the diffusion of Cr is eliminated. Some Fe diffusion is observed from the cathode to the MC.
2) XPS analysis confirms that there are more Cr deposits on the cathode surface in contact with the uncoated alloy than with the coated alloys. The results confirm that the secondary phases of Cr_2O_3 and $SrCrO_4$ are formed. A substantial decrease in the Cr 2p peak intensities was observed in the coated metallic interconnects, indicating that the reactivity is decreased.
3) The application of MC and MCF10 spinel as protective coatings not only results in a significant decrease in the contact resistance between the LSF40 cathode and the stainless steel interconnects (Crofer 22 APU, SS430 and Conicro 4023 W 188), but also acts as an effective barrier to the outward diffusion of Cr cations into the cathode material.
4) The MCF10 is a more effective barrier than MC, resulting in better electrochemical results and a similar microstructure after 800 °C for 100 h in air. The presence of a low Fe content in the MCF10 improves the conductivity and stability of these oxides.

This study demonstrates that the MCF10 coating is a promising material to be used as a protective layer for a material with approximately 22% Cr weigh and other reactive elements (La, Mn, and Si), such as Crofer 22 APU and Conicro 4023 W 188.

Acknowledgements

This work has been financially supported by the Ministerio de Ciencia e Innovación (MAT2010-15375 and Consolider-Ingenio

2010 CSD2009-00013), the Consejería de Industria, Innovación, Comercio y Turismo of the Basque Government (SAIOTEK 2012 programme) and the Consejería de Educación, Universidades e Investigación of the Basque Government (IT-177-07). The authors wish to thank Ikerlan's Fuel Cell group (Miñano, Álava) and the technical and human support provided by SGIker (UPV/EHU, MICINN, GV/EJ, ESF). V. Miguel-Pérez wishes to thank UPV/EHU for funding her PhD work.

References

[1] S.C. Singhal, K. Kendall, High Temperature Solid Oxide Fuel Cells: Fundamentals, Design and Applications, Elsevier, Ltd., Oxford, UK, 2003.
[2] A. Martínez-Amesti, "Celdas de Combustible de Óxido Sólido. Estudios de Reactividad y Optimización de la Intercapa Cátodo-Electrolito", UPV/EHU, Leioa, Spain, 2009. Ph. D. Thesis.
[3] N. Sammes, Y. Du, "Full Cell Technologies: State and Perspectives", Springer, Netherlands, 2005, pp. 19–34.
[4] A.J. Jacobson, Chem. Mater. 22 (2010) 660–674.
[5] A. Martínez-Amesti, A. Larrañaga, L.M. Rodríguez-Martínez, A.T. Aguayo, J.L. Pizarro, M.L. Nó, A. Laresgoiti, M.I. Arriortua, J. Power Sources 185 (2008) 401–410.
[6] J.W. Fergus, Solid State Ionics 171 (2004) 1–15.
[7] C. Johnson, N. Orlovskaya, A. Coratolo, C. Cross, J. Wu, R. Gemmen, X. Liu, Int. J. Hydrogen Energy 34 (2009) 2408–2415.
[8] K. Hilpert, W.J. Quaddakers, L. Singheiser, in: W. Vielstich, H.A. Gasteiger, A. Lamm (Eds.), Handbook of Fuel Cells – Fundamentals, Technology and Applications vol. 4, John Wiley & Sons, New Jersey, USA, 2003, pp. 1037–1051.
[9] W.Z. Zhu, S.C. Deevi, Mater. Sci. Eng. A348 (2003) 227–243.
[10] J.W. Fergus, Mater. Sci. Eng. A397 (2005) 271–283.
[11] J. Wu, X. Liu, J. Mater. Sci. Technol. 26 (4) (2010) 293–305.
[12] V. Miguel-Pérez, A. Martínez-Amesti, M.L. Nó, A. Larrañaga, M.I. Arriortua, Corros. Sci. 60 (2012) 38–49.
[13] Z. Yang, G. Xia, P. Singh, J.W. Stevenson, J. Power Sources 155 (2006) 246–252.
[14] T. Horita, Y. Xiong, H. Kishimoto, K. Yamaji, M.E. Brito, H. Yokokawa, J. Electrochem. Soc. 157 (5) (2010) B614–B620.
[15] J.W. Fergus, Int. J. Hydrogen Energy 32 (2007) 3664–3671.
[16] K. Wang, J.W. Fergus, J. Electrochem. Soc. 157 (2010) B1008–B1011.
[17] N. Shaigan, W. Qu, D.G. Ivey, W. Chen, J. Power Sources 195 (2010) 1529–1542.
[18] Q. Fu, F. Tietz, D. Sebold, E. Wessel, H.-P. Buchlremer, Corros. Sci. 54 (2012) 68–76.
[19] W. Qu, L. Jian, D.G. Ivey, J.M. Hill, J. Power Sources 157 (2006) 335–350.
[20] E. Konysheva, J. Laatsch, E. Wessel, F. Tietz, N. Christiansen, L. Singheiser, K. Hilpert, Solid State Ionics 177 (2006) 923–930.
[21] X. Xin, S. Wang, Q. Xhu, Y. Xu, T. Wen, Electrochem. Commun. 12 (2010) 40–43.
[22] M.R. Bateni, P. Wei, X. Deng, A. Petric, Surf. Coat. Technol. 201 (2007) 4677–4684.
[23] Z. Yang, G.-G. Xia, X.-H. Li, J.W. Stevenson, Int. J. Hydrogen Energy 32 (2007) 3648–3654.
[24] L. Chen, E.Y. Sun, J. Yamanis, N. Magdefrau, J. Electrochem. Soc. 157 (6) (2010) B931–B942.
[25] E. Àlvarez, A. Meier, K.S. Weil, Z. Yang, Int. J. Appl. Ceram. Technol. 8 (2011) 33–41.
[26] C.C. Mardare, M. Spiegel, A. Savan, A. Ludwig, J. Electrochem. Soc. 156 (2) (2009) 1431–B1439.
[27] X. Montero, F. Tietz, D. Sebold, H.P. Buchkremer, A. Ringuede, M. Cassir, A. Laresgoiti, I. Villarreal, J. Power Sources 184 (2008) 172–179.
[28] K. Wang, Y. Liu, J.W. Fergus, J. Am. Ceram. Soc. 94 (2) (2011) 4490–4495.
[29] H.M. Rietveld, Acta Crystallogr. 22 (1967) 151–152.
[30] H.M. Rietveld, J. Appl. Crystallogr. 2 (1969) 65–71.
[31] J. Rodríguez-Carvajal, Fullprof, "Rietveld Pattern Matching Analysis of Powder Patterns", Grenoble, 1994.
[32] C.-L. Chu, J.-Y. Wang, S. Lee, Int. J. Hydrogen Energy 33 (2008) 2536–2546.
[33] R.-H. Jung, H. Tsuchiya, S. Fujimoto, Corros. Sci. 58 (2012) 62–68.
[34] J.L. Gautier, S. Barbato, J. Brenet, C.R. Acad. Sci. Paris 294 (1982) 427–430.
[35] A. Martínez-Amesti, A. Larrañaga, L.M. Rodríguez-Martínez, M.L. Nó, J.L. Pizarro, A. Laresgoiti, M.I. Arriortua, J. Power Sources 192 (2009) 151–157.
[36] J. García, G. Subías, J. Phys. Condens. Matter. 16 (2004) 145–178.
[37] E. Rios, P. Lara, D. Serafini, A. Restovic, J.L. Gautier, J. Chil. Chem. Soc. 55 (2) (2010) 261–265.
[38] A. Hagen, J. Östby, Oxidation states of Mn, Cr, and Co in Mixed Spinels Studied by XANES, Ed. U. Bossel, in: Proceeding Oberrohrdorf: European Fuel Cell Forum, 2006.
[39] H.J. Lee, G. Kim, D.H. Kim, J.-S. Kang, C.L. Zhang, S.-W. Cheong, J.H. Shim, S. Lee, H. Lee, J.-Y. Kim, B.H. Kim, B.I. Min, J. Phys. Condens. Matter. 20 (2008) 1–5.
[40] M.R. Siddiquah, "Effect od Doping of Varios Metal Cations on Structural Electrical and Magnetic Properties of Nano Cobalt Ferrites", Quaid-I-AZAM University, Islamabad, 2008. Ph. D. Thesis.
[41] R.D. Shannon, Acta Crystallogr. Sec., A 32 (1976) 751–767.
[42] B. Hua, J. Pu, W. Gong, J. Zhang, F. Lu, L. Jian, J. Power Sources 185 (2008) 419–422.
[43] Y. Fang, C. Wu, X. Duan, S. Wang, Y. Chen, Int. J. Hydrogen Energy 36 (2011) 5611–5616.
[44] V. Miguel-Pérez, A. Martinez-Amesti, A. Larrañaga, M.L. Nó, M.I. Arriortua, "Reduction of Cathode Degradation from SOFC Metallic Interconnects by MnCo2O4 Spinel Protective Coating", in: Proceedings of the 10th European SOFC Forum, 26–29 Jun, Lucerne, Switzerland, 2012.
[45] A. Machet, A. Galtayries, P. Marcus, P. Combrade, P. Jolivet, P. Scoot, Surf. Interface. Anal. 34 (2002) 197–200.
[46] A.N. Hansson, S. Linderoth, M. Mogensen, M.A.J. Somers, J. Alloys Compd. 433 (2007) 193–201.
[47] X. Chen, P.Y. Hou, C.P. Jacobson, S.J. Visco, L.C.D. Jonghe, Solid State Ionics 176 (2005) 425–433.
[48] J. Puranen, J. Lagerbom, L. Hyvärinen, M. Kylmälahti, O. Himanen, M. Pihlatie, J. Kiviaho, P. Vuoristo, J. Therm. Spray Technol. 20 (2011) 154–159.